IEEE Access
Multidisciplinary | Rapid Review | Open Access Journal

Received May 17, 2018, accepted June 28, 2018, date of publication July 13, 2018, date of current version August 15, 2018.

Digital Object Identifier 10.1109/ACCESS.2018.2855725

Subsea Pipeline Corrosion Estimation by Restoring and Enhancing Degraded Underwater Images

AMJAD KHAN[1], SYED SAAD AZHAR ALI[1], (Senior Member, IEEE), ATIF ANWER[1], SYED HASAN ADIL[2], AND FABRICE MÉRIAUDEAU[1]

[1]Center for Intelligent Signal and Imaging Research, Electrical and Electronic Engineering Department, Universiti Teknologi PETRONAS, Seri Iskandar 32610, Malaysia

[2]Software Engineering Department, Iqra University, Karachi 75260, Pakistan

Corresponding author: Fabrice Mériaudeau (fabrice.meriaudeau@utp.edu.my)

This work was supported by YUTP-FRG funded by PRF under Grant 0153AA-E52.

ABSTRACT Subsea pipeline corrosion is considered as a severe problem in offshore oil and gas industry. It directly affects the integrity of the pipeline which further leads to cracks and leakages. At present, subsea visual inspection and monitoring is performed by trained human divers; however, offshore infrastructures are moving from shallow to deep waters due to exhaustion of fossil fuels. Therefore, inhospitable underwater environmental conditions for human diver demand imaging-based robotic solution as an alternate for visual inspection and monitoring of subsea pipelines. However, an unfriendly medium is a challenge for underwater imaging-based inspection and monitoring activities due to absorption and scattering of light that further leads to blur, color attenuation, and low contrast. This paper presents a new method for subsea pipeline corrosion estimation by using color information of corroded pipe. As precursor steps, an image restoration and enhancement algorithm are developed for degraded underwater images. The developed algorithm minimizes blurring effects and enhances color and contrast of the images. The enhanced colors in the imaging data help in corrosion estimation process. The image restoration and enhancement algorithm are tested on both experimentally collected as well as publicly available hazy underwater images. A reasonable accuracy is achieved in corrosion estimation that helped to distinguish between corroded and non-corroded surface areas of corroded pipes. The qualitative and quantitative analyses show promising results that encourage to integrate the proposed method into a robotic system that can be used for real-time underwater pipeline corrosion inspection activity.

INDEX TERMS Underwater image, restoration, enhancement, subsea pipeline, corrosion estimation.

I. INTRODUCTION

Subsea pipelines are the backbone in offshore petrochemical industry for transportation of oil and gas to the onshore setup for further chemical processes. In order to ensure the safe and uninterrupted transportation of extracted oil, these underwater pipelines require inspection on a regular basis for corrosion, cracks and leakages. Several methods such as saturation diving, pigging and Underwater Vehicles have been developed to inspect the pipelines to maintain their integrity [1]. Although, the subsea pipelines are manufactured with several protection layers to minimize the external environmental effects, however, with the passage of time, the protection layers get damaged or disbonded by harsh underwater situations. As a result, the water molecules penetrate under the damaged or disbonded layers. The direct contact of water molecules with metallic surface of the pipeline initiates the oxidation process [2]. The oxidation progresses further to corrosion on external surface of the pipeline and affects its integrity by bringing cracks and leakages [3], [4].

In the offshore petrochemical industry, subsea pipeline corrosion is considered as a severe problem. At present, different techniques are being tested to provide better solution for the detection of corroded surface of the pipeline. Corrosion detection helps further to repair the effected surface timely before any catastrophic failure occurs. Since last few years, researchers have been working on non-destructive

2169-3536 © 2018 IEEE. Translations and content mining are permitted for academic research only.
Personal use is also permitted, but republication/redistribution requires IEEE permission.
See http://www.ieee.org/publications_standards/publications/rights/index.html for more information.

testing (NDT) methods to inspect/detect the corrosion on subsea pipeline and monitor its structural health [4]–[6]. Commonly used NDT methods are based on radiographic, electromagnetic, ultrasonic, liquid penetrant testing, magnetic particle, acoustic emission, infrared and thermal and visual testing [7]–[9].

The visual testing (VT) among other NDT methods is considered as most effective due to its simplicity and low cost. In VT method, a trained inspector or engineer equipped with simple tools such as flash light and diving skills is assigned to inspect the subsea pipelines. The VT method can be performed at shallow waters more effectively, however, the offshore infrastructures are now moving from shallow waters to deep waters due to the exhaustion of fossil fuels [10]. In deep waters, the VT method by human inspectors is not only difficult but also increases life risks, labor cost and inspection time due to numerous factors. However, the importance, simplicity and effectiveness of VT method brought alternative robotic solutions for deep waters such as Remotely Operated Vehicle (ROV), Human Occupied Vehicle (HOV) and Autonomous Underwater Vehicle (AUV). These underwater vehicles (UVs) are suitable alternates of human inspectors with higher efficiency and almost zero life risks involved. The UVs are normally equipped with various sensors to collect information during inspection activities [11]–[13]. Among these sensors, the underwater cameras are being used to acquire imaging data. The image/video data can be analyzed further for fault detection and corrosion inspection activities.

In the remainder of the paper, Section 2 discusses the related research that has been done for underwater image enhancement to solve different challenges including corrosion detection, Section 3 describes each step of the proposed methodology for underwater image restoration, enhancement and corrosion estimation. Section 4 discusses the results and performance evaluation of the proposed method. Section 5 presents the concluding remarks with future works.

II. RELATED WORK

The image based corrosion detection techniques have been developed in past few years to perform inspection in different areas, especially where human access is inviable due to environmental and other factors involved [14], [15]. In [16], an image based solution for corrosion detection on the vessel hull is presented. A two stages method is developed using weak classifier color-based corrosion detection algorithm. At the first stage, the algorithm evaluates the corroded surface as rough texture by relating it with the energy calculated by using symmetric gray level co-occurrence matrix (GLCM). At the second stage, the patches of pixels that have passed the first stage are filtered based on their roughness. Then the color information of the corroded patches is observed in HSV color space to distinguish corroded pixels from non-corroded pixels (i.e. black or white pixels).

Another image based inspection approach for detection of cracks and corrosion inside a boiler header is discussed in [17]. The technique is implemented on Laboratory Virtual Instrument Engineering Workbench (LabVIEW). The inspection is performed on a 360-degree view of cross section of boiler header in real time. After image acquisition, segmentation is performed using thresholding technique and the corroded areas are distinguished based on visual analysis that shows the corroded areas that are relatively brighter compared with rest of the scene. Edge detection is performed to get the boundaries information of the corroded regions. A particle analysis is than conducted to find the statistical information such as area, pixel value, location and presence of particles in corroded region. Similarly, imaging based corrosion inspection concept for urban pipeline networks is presented in [18]. The platform comprises on an inspection mobile robot with line laser and a closed-circuit television (CCTV) camera. The inspection task focuses on the inner structure of the pipeline where visual inspection by human is not possible. Besides the width of corroded region and its distance from start point, the method can detect dangerous cracks.

An image based texture analysis for corrosion monitoring is presented in [19]. In this analysis an experiment on ASTM A36 steel for atmospheric corrosion process is conducted. During the experiment, a sequence of image is acquired to test the corrosion evolution over a period of 44 days. From the acquired images six different textural characteristics such as entropy, Hurst coefficient, contrast, correlation, energy and homogeneity are extracted. The image-based analysis presented is feasible to check the state of surface corrosion on ASTM A36 steel materials. Similar approach is discussed in [20] to detect rust zones using images of metals. The rust detection model consists of image acquisition, filtering, feature extraction and classification steps. For the performance evaluation of the model, the acquired images of metals are simulated with the Perlin noise in order to get different levels of corrosion, including extreme rust conditions.

In order to develop image-based corrosion inspection solutions for underwater situations, there are various preprocessing steps involved due to environmental effects on image formation process. The underwater image formation process faces light absorption and scattering problems by the presence of suspended particles in turbid water. The light scattering, and absorption further lead to blur, color attenuation and low contrast issues on the image data acquired in an underwater environment. Therefore, for any VT based corrosion inspection task using UVs, it is essential to improve the quality of the image/video data by minimizing the blur, color attenuation and low contrast issues. In recent years, various image enhancement and dehazing methods have been developed for numerous underwater activities.

Chiang and Chen [21] have tackled the underwater image haze issue by estimating depth maps (i.e. distances between camera and objects) and by segmentation of foreground and background. They also determined the presence or absence of an artificial light source in the image that needs to be removed or compensated. The depth maps in an image are perceived using stereo or parallax images. However, the authors note that since haze increases with distance, therefore, haze is

a useful clue for understanding the depth of the scene, by evaluating the concentration of haze in an image between objects. Next, the absence or presence of artificial light in the image is detected by comparing the difference between the mean luminescence of the foreground and background. In an underwater image, higher foreground means luminescence which indicates the existence of a supplementary light source and can be removed. Next, the presented method shows the removal of haze by compensation of light scattering and color changes along the object camera path by removing the scattering model from the image formation model perceived by the camera. Then estimation of underwater depth in each pixel of the image is presented. Once the depths at each pixel have been estimated, the restored energy of the image can be modified for better color correction after haze removal.

Li and Guo [22] have proposed an approach that utilizes a simple de-hazing technique coupled with color compensation, histogram equalization followed by stretching in saturation and intensity in the HSI planes. The proposed method results in improved contrast, visible and brighter underwater images. For dehazing, the authors have proposed a simplified underwater hazy image formation model to estimate the medium transmission map and global atmospheric light. Finally, a bilinear filter is applied to de-noise the image that results in much clear image features.

Cheng *et al*. [23] presented the underwater image restoration based on red-dark channel prior and point spread function deconvolution. McGlamery [24] and Jaffe [25] simplified the Jeff- McGlamery optical image formation model and proposed an effective algorithm to recover the degraded underwater images. The red-dark channel is derived to estimate the background light and the transmission. The visibility of the scene is also compensated by the depth information to recover the colors of the background as well as of the object. An efficient low pass filter is developed from the analysis of point spread function presented in Jaffe-McGlamery model [24], [25]. This filter is then used in deconvolution process to deblur degraded underwater images.

In an underwater environment, the absorption of light in water varies with the wavelengths. As red color is the earliest to attenuate, the underwater images offer lower contrast and exhibit color distortion. In [26], a red channel method is proposed, as a variant of the dark channel method [27] (scene depth derivation based on observation of background light patches on haze free underwater images) for recovering the colors associated with the shorter wavelengths, thus recovering and improving the low contrast and restoring a natural color. Since it is assumed that the degradation is related to the distance of the object from the camera, the color of the water is first estimated using the assumed farthest pixel in the image. Then the transmission of the scene is estimated on each of the RGB components of the image, even though the three matrices are dependent. Since artificially illuminated images in water are common, the presented method accommodates the saturation component for a proper color correction of the images.

An underwater image restoration based on image blurriness and light absorption is presented in [28]. The authors used image blurriness and light absorption to estimate the background light, scene depth, and transmission maps and tested on both synthesized and real underwater images with different color tones and contents.

Li *et al*. [29] developed a physical model for underwater imaging and presented a fine dust removal technique based on deep convolutional neural networks. In another work by Lu *et al*. [30], the authors proposed a hierarchical transmission fusion method and a color-line ambient light estimation method for image de-scattering from a single input image. They estimated the preliminary transmission and ambient light by taking dark channel as prior information. Then they used color lines to estimate the refined ambient light in selected patches obtained the final transmission by a joint normalized filter. The final scene color was achieved by applying color correction and de-blurring.

Ancuti *et al*. [31], [55], and [59] have investigated underwater image enhancement using different techniques. In [31], a multiscale implementation of the fusion of contrast corrected and white balanced version of image resulted in artifact-free blend for underwater image enhancement. The technique was based on single image for several challenging underwater environments. A review of intelligent underwater image dehazing and color restoration is presented in [32].

This paper contributes to subsea pipeline corrosion estimation by restoring and enhancing the degraded underwater images. Firstly, the developed methodology for underwater image restoration and enhancement is discussed. The methodology is used to minimize the underwater effects on image such as blur, color attenuation and low contrast. Secondly, the corrosion estimation is presented on different patterns of corroded surface of pipe that were acquired in an underwater environment. The region of interest is clustered into three distinct clusters (i.e. non-corroded, low-corroded and high-corroded) based on color information using unsupervised clustering technique. The degree of corrosion in each corroded pattern is calculated in terms of percentage of pixels count in each cluster with respect to region of interest.

III. UNDERWATER IMAGE ACQUISITION, RESTORATION, ENHANCEMENT AND CORROSION ESTIMATION

The proposed methodology presented in this study is given in FIGURE 1. Initially the acquired hazy or blurred underwater image is processed to segment the region of interest. Then the blurring parameters are estimated on segmented region and based on estimated blurring kernel, the image is restored or deblurred. Afterwards, the color and contrast are enhanced. Then, both enhanced versions are fused into a restored and enhanced image. Finally, the restored and enhanced region of interest is grouped into three different clusters to estimate the corrosion in terms of percentage of pixels in the corroded region.

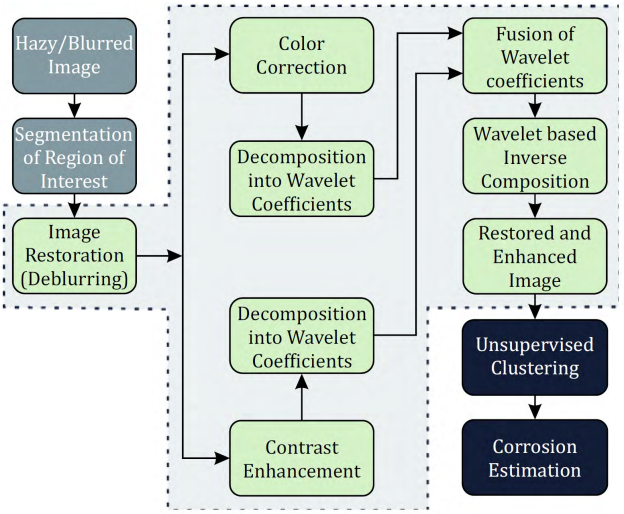

FIGURE 1. Proposed methodology for underwater image restoration, enhancement and corrosion estimation.

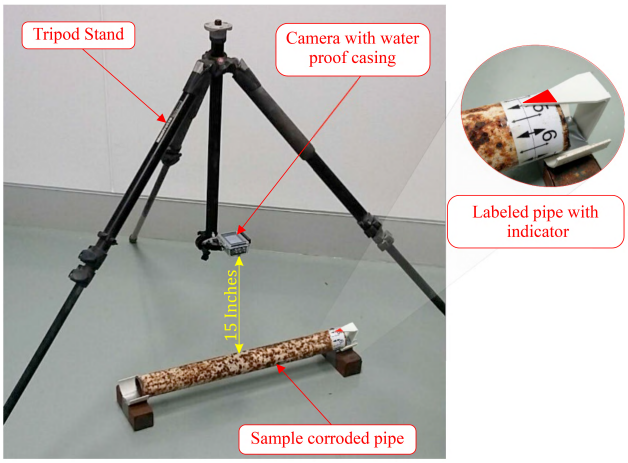

FIGURE 2. Designed experiment setup for underwater image acquisition.

A. IMAGE ACQUISITION AND PRE-PROCESSING

1) IMAGE ACQUISITION SETUP

The experiment setup designed for image acquisition is shown in FIGURE 2. Corroded pipes with different corrosion patterns were used in the image acquisition process. These pipes were labeled, and each pipe was divided into eight equal surfaces. An indicator was designed and printed using 3D printing facility. This indicator helped to get the exact surface position in the underwater environment while rotating the pipe from one surface to the other. During the setup calibration, the distance from the camera to the pipe was kept constant at 15 inches. The image acquisition was performed using Novatek SJ5000 sports action (14MP) camera by SJCAM with a waterproof casing. For underwater image acquisition, the offshore laboratory facility available within the university premises was used. The offshore laboratory consists of wave-tank with the dimensions

FIGURE 3. (a) UTP offshore lab facility and (b) experiment setup calibration in an underwater environment.

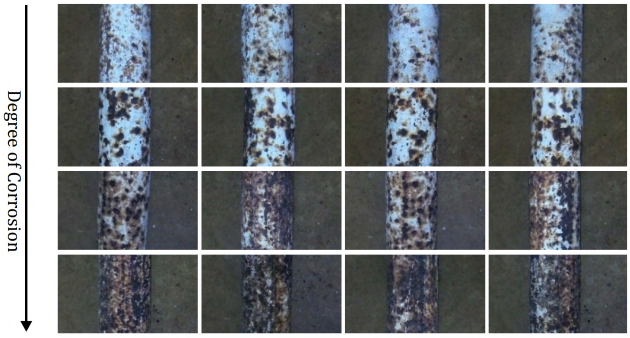

FIGURE 4. A set of acquired underwater images of different corrosion patterens arranged per degree of corrosion.

of 20×10×1 (Length × Width × Height) meters as shown in FIGURE 3(a). The designed experiment setup was installed and calibrated in the wave tank. An artificial light source of 80 Lumens consists of 10 cool white LEDs was used to illuminate the underwater scene. In FIGURE 3(b), the image acquisition setup is shown during image data acquisition in an underwater condition.

In the wave tank, the underwater imaging process was simulated such that it could emulate the real underwater inspection process. During image acquisition, 237 images of corroded pipes with different patterns and degree of corrosion were captured. The images were cropped to a dimension of 1280×720 pixels. Some sample images from the acquired dataset of corroded pipes with different degree of corrosion are shown in FIGURE 4.

2) SEGMENTATION OF REGION OF INTEREST

The segmentation is a major step in the proposed methodology that does not only help to segment the required object from the image but also reduces the computational cost in further image enhancement steps. Instead of processing the whole image only the region of interest (ROI) is considered. To segment the required ROI, an entropy-based segmentation is implemented. Entropy of the image gives information about the textures contained in an image. Since in acquired database the focus is on the pipes, therefore, by determining the entropy of the images, the texture of the pipe from the image can be obtained. The textural information helps to

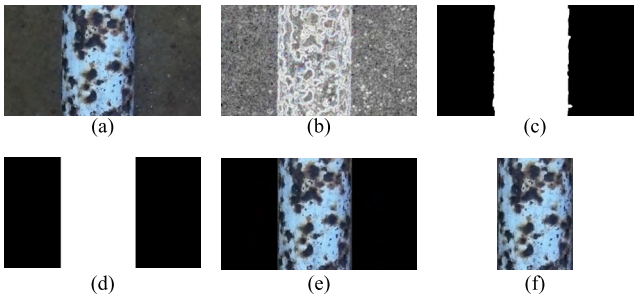

FIGURE 5. The segmentation of region of interest (a) original image with corroded pipe (b) entropy based rescaled gray image (c) generated binary mask from rescaled image (d) binary mask with smoothed edges (e) segmented pipe with full dimensions (f) final segmented pipe by removing false pixels.

develop a binary mask which is further used to extract the pipe from the original RGB image.

The entropy $H(p)$ is a statistical quantity of randomness of the pipe image which is used to predict the texture at each pixel of the image as given by the Eqn.(1).

$$H(p) = -\sum_x p(x) \log_2 p(x) \tag{1}$$

where $p(x)$ is the distribution of intensity in different color components of the image and logarithm is taken on base 2. In a color image, different texture has different distribution of color intensity. By using this technique, the entropy value of each 9-by-9 neighborhood around the corresponding pixel in the image is calculated. Then the entropy values of all pixels are rescaled into grayscale image. From textural information of the rescaled image, a binary mask is generated to segment the ROI. An estimated projection from binary mask is applied to refine the edges.

Finally, this binary mask is used to segment the pipe in the RGB image. The entropy of the original image as shown in FIGURE 5(a) is calculated to get the textural information. The textural information is then rescaled to a gray image as shown in FIGURE 5(b). From the gray image, the binary mask as illustrated in FIGURE 5(c) is generated with the help of morphological operations. During segmentation, it is observed that the outer edges of the binary mask are not smooth that makes it difficult to segment the pipe properly. Therefore, a projection is estimated by taking the average of the true pixels vertically on both outer edges of the binary mask in the image plane. Then the estimated projection is applied to the binary mask to smooth its edges by removing outlier pixels as given in FIGURE 5(d). Finally, the binary mask is used to segment the corroded pipe from the original image which is shown in FIGURE 5(e). In order to obtain the only pixels that are the part of the region of interest, the remaining false/black pixels are removed as shown in FIGURE 5(f). By following the above steps, all captured images are passed through the segmentation to get the region of interest.

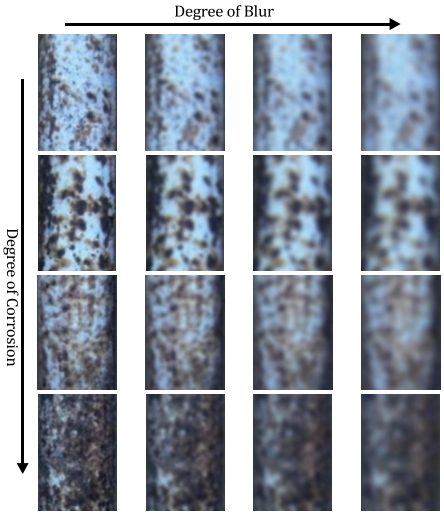

FIGURE 6. A set of segmented images with different degree of blur and corrosion.

3) SIMULATED BLUR

The Gaussian blur is a common phenomenon for underwater imaging due to dispersion of light [33] and hydrodynamic disturbances even in clear or less turbid water. Due to the limitation of depth and less turbid water in the experimental lab, the acquired images have unnatural degradation effects.

Therefore, the environmental effects are simulated by inducing the Gaussian blur artificially (using different values of σ_{sim}) as shown in FIGURE 6. The detailed description of inducing Gaussian blur in self-acquired underwater image dataset is mentioned in [34]. The simulated blur helped to keep the ground truth images same for different blurring levels which is not possible in the images that are acquired even in real blurry environment of the same underwater location. The blurred images are divided into four groups based on blurring level from Group 1 (low blur) to Group 4 (extreme blur).

B. IMAGE RESTORATION AND ENHANCEMENT

The underwater images are mostly blurred due to turbid medium. Mathematically, a blurred image can be approximately described by the Eqn.(2).

$$b(x, y) = (h * o)(x, y) + n(x, y) \tag{2}$$

where $b(x, y)$ is the blurred image, $h(x, y)$ is the point spread function (PSF) or distortion operator present in the original image, $o(x, y)$ and $n(x, y)$ are additive noise that comes from the medium during image capturing process. Based on this model, the ultimate task of deblurring is to de-convolve the blurred image with the PSF that exactly describes the distortion. PSF is required to be estimated to perform deconvolution process, therefore, the standard deviation σ_{est} of the deblurring kernel is estimated first to calculate PSF. The estimation of σ_{est} is performed with the help of an artificial neural network (ANN). In the proposed method, the ANN fitting tool with the sigmoid function is used to train the network.

The input data consists of features of the image whereas the values of standard deviation of the simulated blurring kernel in the image is given as a target or output. For feature vector, seven distinctive features of each image are selected by analyzing their tendencies in the image dataset. These features include contrast, correlation, energy, homogeneity, range, entropy and standard deviation. Then a vector is developed by extracting these features from all simulated images. Similarly, a target vector is created by gathering the value of standard deviation of blurring kernel against each image. Before training, both input and target vectors are normalized. In order to estimate the σ_{est}, AAN training is performed using 70% of the fetched data while 30% of the data is used to validate and test the module. After ensuring better performance in training, validation, and testing, a model is obtained. Then features of each blurred image are extracted, normalized and passed through the model. By de-normalizing the output, an estimated σ_{est} for the deblurring kernel of the input image is obtained. The process is repeated for all blurred images to estimate σ_{est} and then to calculate deblurring kernel or PSF for deconvolution process. Here deblurring kernel is denoted by σ_{est} and is given in the Eqn. (3).

$$g(x, y) = \frac{1}{2\pi\sigma_{est}^2} e^{-\frac{x^2+y^2}{2\sigma_{est}^2}} \tag{3}$$

In order to complete the image restoration process, the Wiener filter-based deconvolution is used. In Wiener deconvolution, the blurred image $b(x, y)$ which is given in Eqn. (2), is convolved with estimated deblurring kernel $g(x, y)$ to obtain restored image $\hat{o}(x, y)$ as given in the Eqn.(4).

$$\hat{o}(x, y) = g(x, y) * b(x, y) \tag{4}$$

The Wiener deconvolution filter provides $g(x, y)$ in the frequency domain as given by [35] the expression in Eqn.(5).

$$G(u, v) = \frac{1}{H(u, v)} \left[\frac{[H(u, v)]^2}{[H(u, v)]^2 + \frac{1}{SNR(u,v)}} \right] \tag{5}$$

where $G(u, v)$ and $H(u, v)$ are, the Fourier transforms of $g(x, y)$ and $h(x, y)$ respectively at locations (u, v) in frequency domain, $SNR(u, v)$ is the signal to noise ratio. The deconvolution operation is carried out either as shown in Eqn. (4) or in frequency domain as given in Eqn. (6) [35].

$$\hat{O}(u, v) = G(u, v) \times B(u, v) \tag{6}$$

$\hat{O}(u, v)$ and $B(u, v)$ are the Fourier transforms of restored image $\hat{o}(x, y)$ and blurred image $b(x, y)$ respectively and by performing inverse Fourier transform on $\hat{O}(u, v)$, the restored image $\hat{o}(x, y)$ is obtained. In Wiener deconvolution, SNR is calculated as a ratio of the variance of blurred image to the variance of noise. In the simulated data, the blur is induced through a low pass filter that already has suppressed the noise to a negligible state, therefore variance of noise is considered as low as to 0.0001. However, for real images the variance of noise can be calculated on the noise component. In order to obtain the noise component, a low pass filter with neighborhoods of size 3-by-3 is applied to the blurred image which results in a filtered component, the subtraction of filtered component from the blur image gives the noise component. Then the estimated blurring kernel and SNR are used in Weiner deconvolution process to restore original features of the blurred images. All blurred images are passed through the explained restoration process. FIGURE 7, shows a few sample restored images with their estimated values of σ_{est}.

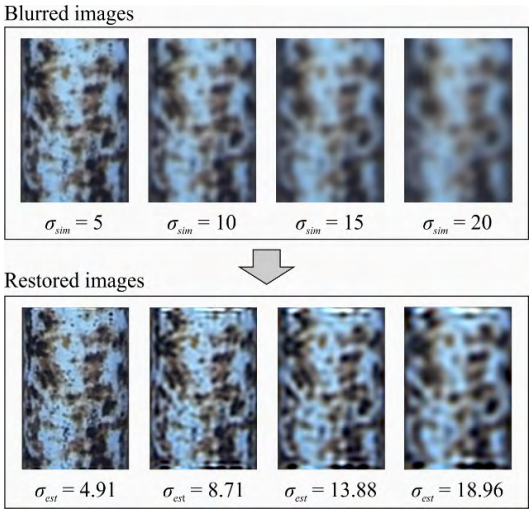

FIGURE 7. An image with different blurring levels and its restored versions with ANN based estimated values of σ_{est} for Wiener deconvolution.

Upon restoration, the segmented image of the corroded pipe is further passed through the color correction process. For color correction, the image is converted from RGB (Red-Green-Blue) to HSV (Hue-Saturation-Value) color space. In HSV color space, the histogram of the Value component is stretched over the entire range. This improves the brightness of the available colors in the image. Then the Hue and Saturation are concatenated with the corrected Value component, and then the image is converted back to the RGB color space. In RGB color space, once again the histogram is stretched over the whole intensity range (0 to 255) to achieve the color correction in all three channels. The histogram stretching is based on the mathematical expression given by Ghani and Isa [36] in the Eqn. (7).

$$P_{out} = (P_{in} - i_{\min}) \left(\frac{o_{\max} - o_{\min}}{i_{\max} - i_{\min}} \right) + o_{\min} \tag{7}$$

where P_{out} and P_{in} are the pixels of output and input images respectively. $i_{\min}$, $i_{\max}$, $o_{\min}$ and $o_{\max}$ are minimum and maximum values of intensities for input and output images respectively.

The absorption of light reduces the contrast in underwater images and makes the image features dull. This condition reduces the possibility to recognize the required objects by the vision system during underwater inspection task. In order to enhance the contrast of the underwater images,

Contrast Limited Adaptive Histogram Equalization (CLAHE) is adopted [37]. The CLAHE is a variant of Adaptive Histogram Equalization (AHE) [38], [39]. In AHE the noise over-amplification tendency is higher during the contrast enhancement. Therefore, to reduce this problem, a contrast limit is defined in CLAHE to clip the unnecessary region from the histogram [40]. The clipping limit is defined by the normalization of the histogram and thereby the size of the neighborhood region in the pixel domain. The clipping region is not discarded but redistributed equally among all histogram bins. The redistribution will push some of the bins over the defined clip limit again, this effect can be reduced by repeating the procedure recursively until the excessive area is negligible. In the proposed method, the CLAHE is applied to all three-color channels in RGB color space separately to enhance the contrast of all available tints in the image.

After enhancing both color and contrast, wavelet based fusion algorithm [41] is used to fuse both color corrected and contrast enhanced images into a single restored and enhanced image. There are various variants of wavelet that are available for multispectral image analysis. However, Daubechies wavelet (db2) is selected among different wavelet types due to its better performance reported by Medina-Daza *et al.* [42] and Park *et al.* [43] for image fusion. Both enhanced images: the color corrected, and the contrast enhanced versions are decomposed into detail and approximate wavelet coefficients (approximate, vertical detail, horizontal detail, and the diagonal detail) using two-level-2D decomposition method. After decomposition of both color corrected and contrast enhanced images, the coefficients are fused together. In the wavelet decomposition, the maximum values of the coefficients contain the higher frequencies or striking features of the image. To fuse the coefficients from both images, the approximate and detail coefficients with maximum values are considered for fusion. After combining coefficients of both enhanced images into fused coefficients, inverse composition is applied to get the synthesized image. For inverse composition, the reverse process is carried out to get a restored and enhanced image. Since, digital image processing deals with discrete data sets; therefore, each input image is decomposed into its coefficients and inversely composed into a synthesized image using discrete wavelet transform (DWT) and inverse discrete wavelet transform (IDWT) respectively. In FIGURE 8, a complete picture of discrete wavelet-based decomposition, fusion and inverse composition of enhanced images is shown.

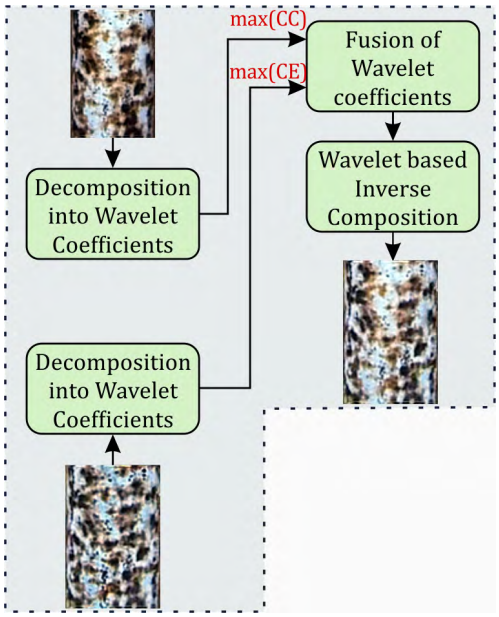

FIGURE 8. Wavelet based-decomposition, fusion and inverse composition of color corrected and contrast enhanced images.

C. CORROSION ESTIMATION

Upon image restoration and enhancement operations, the images are processed further to detect and estimate the corrosion on the surface of the pipes. Before corrosion detection, it is important to describe the distinct levels of corrosion. From the study of underwater oxidation process [44], it is found that normally on metallic objects, the corrosion process does not start uniformly all over the metal surface at the same time. An affected metallic surface can be classified into two major regions: corrosive and non-corrosive. The corrosive region can further be classified into moderate and highly corroded areas. These moderately and highly corroded regions are useful to describe the degree of the corrosion within the region of the interest. This information can be further used to categorize highly affected or damage points on the surface of the pipeline.

In image-based corrosion inspection, color of the corrosion is an important feature to detect the corroded areas and evaluate the degree of corrosion. Therefore, k-means clustering is used to group the pixels of the corroded pipe into three different clusters based on colors. In this study, the original pipelines were white (or white painted), therefore, the white color represents the non-corrosive region while light brown and dark-brown colors are classified as moderate and high corroded areas.

The k-means or Lloyd's algorithm [45] is an iterative process to partition some observations in a dataset into clusters in which each observation belongs to the cluster with the nearest mean. Therefore, k-means algorithm is useful to make the cluster of the corrosion in underwater images of the pipeline. In the proposed method, k-means is used to make the color-based clusters of the corroded pipe. This technique is useful to differentiate the corrosive and non-corrosive areas as well as to assign the levels of the corrosion in the same image. Initially, the restored and enhanced image is converted from RGB to *CIELab* color space. In *CIELab* color space all perceivable colors are described in three dimensions L for lightness, a and b for color opponents. The values of L from 0 to 100 represent the darkest black to brightest white respectively. The red and green opponent colors are represented along a, with green at negative a values and red at positive a values. The yellow and blue opponent colors are

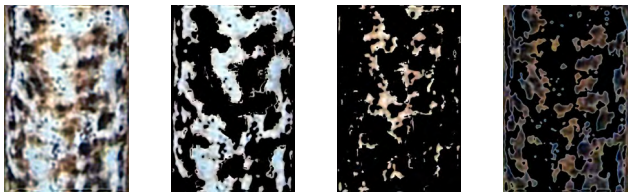

FIGURE 9. k-means based cluster of region of interest of (a) restored and enhanced image into (b) non-corroded, (c) moderately corroded and (d) highly corroded clusters.

represented along the b, with blue at negative b values and yellow at positive b values. Since colors information exists in a and b oponents therefore the difference between two colors can be measured using distance metric in a and b oponents. In proposed method, Euclidean distance is calculated to distinguish three different clusters based on white, light brown and dark-brown colors. Based on Euclidean distance, the pixels are separated into three clusters then each pixel is labeled according to its cluster. The pixels of each cluster are separated from original image.

The k-means clustering technique separates the pixel information of each restored and enhanced image into three clusters based on white, light brown and dark-brown colors as shown in FIGURE 9. The light brown and dark-brown clusters represent the corroded section while white cluster is considered as non-corroded area in the region of the interest. The number of the pixels are calculated in all three clusters. The pixel counts in each cluster is converted into percentage by using the total pixels contained by the region of interest. The percentage of pixels in each corroded cluster points out the moderately and highly corroded regions on the surface of the pipeline during inspection. Similar information of the non-corroded cluster differentiates between affected and healthy regions of pipeline. From moderately and highly corroded clusters, the degree of corrosion can also be approximated within the specific region of interest.

IV. RESULTS AND DISCUSSIONS

The acquired underwater images are processed through each step as described in the proposed methodology. Apart from processing self-collected data the proposed method is also validated on publicly available underwater images that are severely degraded by blur, color attenuation and low contrast issues. In order to evaluate the performance, the statistical quantities of quality evaluation metrics are calculated. For color enhancement evaluation, a color difference metric experiment is also conducted. In the following subsections, the performance of the proposed method along with quality evaluation metrics and color difference evaluation experiment is described in detail.

A. IMAGE QUALITY EVALUATION METRIC

The performance of the proposed method is evaluated using image quality evaluation metrics. The image quality evaluation metric is an important measure to test the quality of a processed image with respect to original image. In this study two quality evaluation metrics namely Full Referenced and Visible Edges Based metrics are used. The quantities of each quality metric with mathematical description and acceptable range or value are given in the following subsections.

1) FULL REFERENCED QUALITY EVALUATION METRICS

The full referenced quality evaluation metric uses the original image as a reference to assess the quality of the processed image. In this study, the metric consists of four quantities namely as Mean Squared Error (MSE), Peak Signal to Noise Ratio (PSNR), Structural Similarity Index Measure (SSIM) and a Measure of Entropy (MoE). The metric is useful to observe the loss of information during image processing operations. If a reference image $r(x, y)$ is compared with a processed image $p(x, y)$ provided that both images have a same size $[n_x, n_y]$ then MSE and PSNR can be formulated as given in Eqn. (8) and Eqn. (9) [46]. The metrics (MSE and PSNR) are calculated in each component of the color image and then mean values of three components (Red Green Blue) are considered for evaluation. The lower MSE and higher PSNR represent improved quality of the processed image.

$$MSE = \frac{1}{n_x n_y} \sum_{0}^{n_x-1} \sum_{0}^{n_y-1} [r(x, y) - p(x, y)]^2 \tag{8}$$

$$PSNR = 10 \log_{10} \left[\frac{\max(r(x, y))^2}{MSE} \right] \tag{9}$$

Similarly, SSIM assess the visual impact of an image using comparison of three characteristics: luminance $[l(r, p)]$, contrast $[c(r, p)]$ and structure $[s(r, p)]$. The overall index can be measured by calculating the multiplicative combination of three terms [47].

$$SSIM_1(r, p) = [l(r, p)]^{\alpha} [c(r, p)]^{\beta} [s(r, p)]^{\gamma} \tag{10}$$

where α, β and γ are parameters used to correct the relative importance of the luminance, contrast and structure respectively and their values are defined as 1. The r and p are the reference and processed images respectively. A detailed mathematical derivation of all three characteristics of SSIM (i.e. luminance, contrast and structure) is formulated in [47] and [48]. The mean SSIM is calculated on a color image with respect to reference image at each pixel as defined in [47] and given by the following expression.

$$SSIM[r, p] = \frac{1}{M} \sum_{j=1}^{M} SSIM_1(r_j, p_j) \tag{11}$$

where r_j and p_j are the image contents of reference and processed images respectively at jth local window while M is the total number of local windows present in the image. Likewise, MoE helps to compare the reference image with the processed image by measuring the features enhancement in terms of textural information. MoE of an image is already defined in Eqn. (1) [46]. For an adequate image quality, the acceptable

range of SSIM is considered to be 0.7 to 1 whereas the higher values of MoE depict better image quality.

2) VISIBLE EDGES BASED QUALITY EVALUATION METRIC

The visible edges-based quality evaluation deals with the comparison of images obtained by different tone mapping operators. In this study, the quality of the publicly available dataset is evaluated using the visible edges based metric proposed in [49] and used in [26] and [50]. This quality metric finds that whether the algorithm has recovered the edges that were lost due to the blurring effects. It works by measuring three coefficients that indicate the new visible edges in the restored or deblurred image. The first of these coefficients, e computes the rate of new visible edges in restored image by developing a map on the restored image and then counting the number of edges on the original image n_o and restored image n_r. Mathematically, it is given by [49] as:

$$e = \frac{n_r - n_o}{n_o} \tag{12}$$

The second coefficient r computes the ratio of the gradient r_i in the restored image for each pixel i that belongs to the visible edges n_r. By taking geometrical mean the following expression is obtained as described by [49].

$$r = \exp\left[\frac{1}{n_r}\sum_i \log(r_i)\right] \tag{13}$$

The final coefficient σ determines the number of pixels n_s that are saturated to black or white by the algorithm. The normalized dimensions $(\dim_x, \dim_y)$ of the image are used in the following calculation as given in [49].

$$\sigma = \frac{n_s}{\dim_x \times \dim_y} \tag{14}$$

For e and r coefficients, the higher measured value depicts the better quality of the processed or restored image which undergoes the evaluation process; whereas σ should be close to zero for better restoration with white background having no saturation [26], [49].

3) HUMAN VISUAL PERCEPTION BASED IMAGE QUALITY EVALUATION METRICS

In order to evaluate the enhanced images in terms of color, contrast and blurring, the human visual perception-based image quality evaluation is also performed. Two recently developed metrics, patch-based contrast quality index (PCQI) [51] and underwater color image quality evaluation (UCIQE) [52] are used. The PCQI is general matric for contrast assessment that provides the accurate predictions on human perception of contrast variations with the local contrast quality map. Its ability to perform the contrast quantification with patch-based approach differentiate it from other global contrast evaluation techniques. In PCQI, each image patch is decomposed into mean intensity, signal strength and signal structure components then their perceptual distortion is measured. At the end, the local score for each patch is averaged to obtain on overall score for entire image. The UCIQE is specifically developed for underwater image quality evaluation by quantifying the colorfulness, sharpness and contrast. The machine learning technique is adopted to calculate the coefficients for blurring, color cast and marine snow on a trained model. The weighted average of standard deviation of chroma, contrast of luminance and average of saturation component of CIELAB space with the calculated coefficients provides a score for each image to assess its color, contrast and blurring.

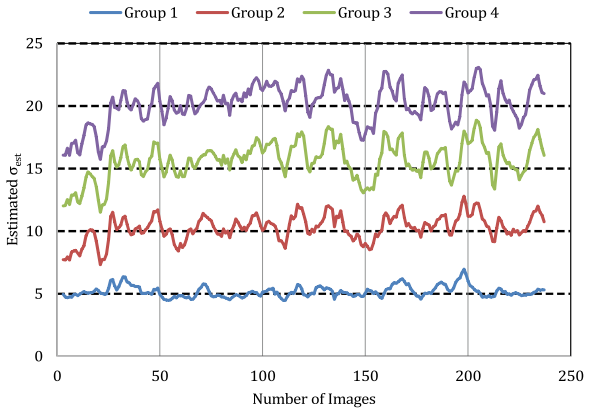

FIGURE 10. Artificial neural network-based estimation of σ_{est} for all four groups of different blurring levels.

B. IMAGE RESTORATION AND ENHANCEMENT

By training a neural network with different distributions of blurred images, it is then used to estimate σ_{est} values for these distributions. In the artificial neural network (ANN) training, the Matlab© NN fitting tool is used to train the data for the estimation of the Gaussian deblurring kernel. For the input of the training algorithm, seven different features from each blurred image are extracted. These features include contrast, correlation, energy, homogeneity, range, entropy and standard deviation. In order to estimate the blurring parameter (σ_{est}) for further calculation of Gaussian point spread function (PSF), the features of 948 images of four groups with different blurring levels are used. Out of these 948 images, 70% are used to train the neural network, 15% for validation and 15% for testing. Each blurring level consists of a set of 237 images. The simulated values of σ_{sim} in each group of images are used as a target vector for the ANN algorithm. In order to obtain the best performance regarding the error, ten hidden layers are used in the ANN training and both input and target values are normalized on a scale of 0 to 1.

After training, validation and testing; a Matlab function is generated and then selected features of each blurred image are passed through this function to obtain the σ_{est}. The results of ANN-based estimation of σ_{est} in each group of blurred images are shown in FIGURE 10. The σ_{est} is approximately estimated for all the images, and its values fluctuat around the desired values with standard deviations of 0.62, 1.37, 1.86 and 1.95 respectively. The mean errors in the estimation for all four groups of different blurred images are obtained

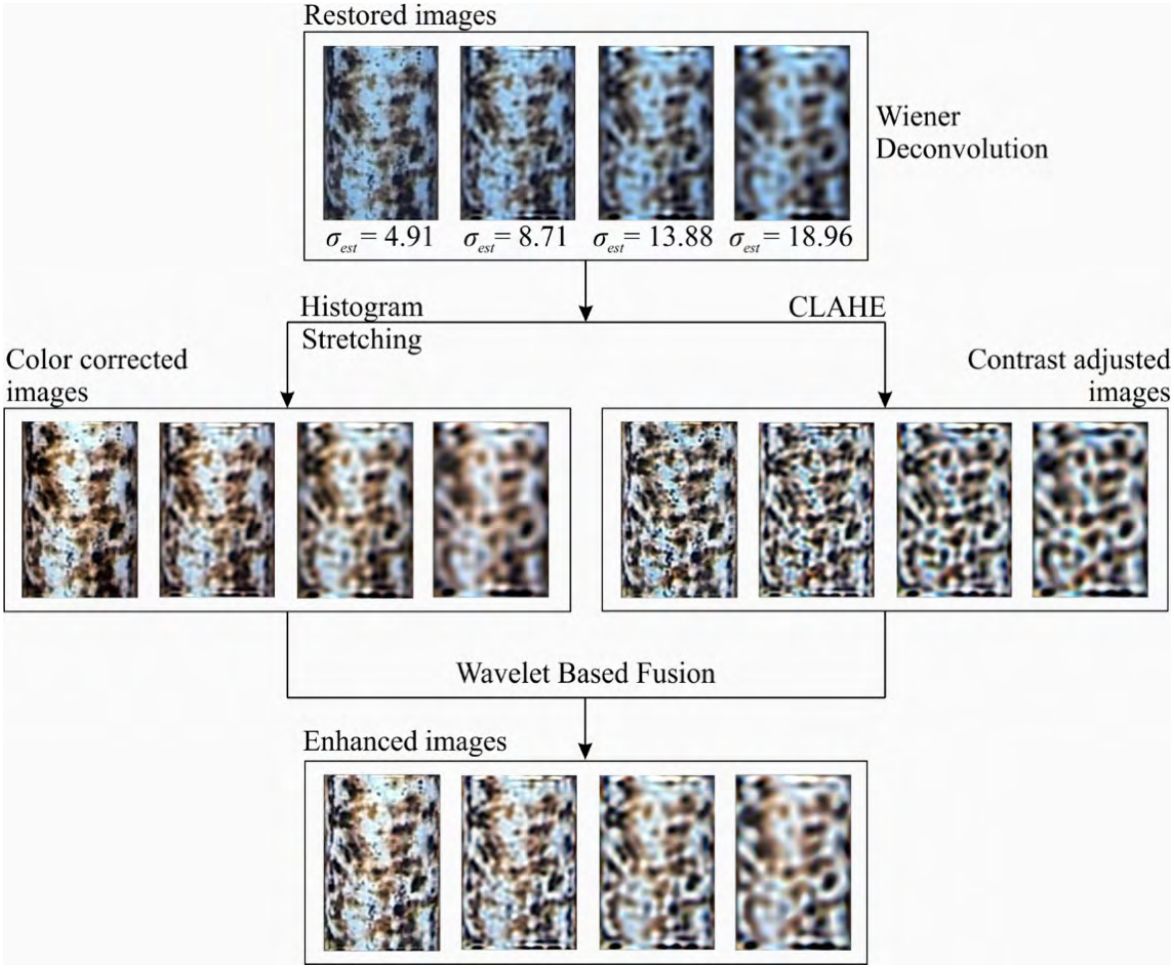

FIGURE 11. Restored images from a different degree of blurring effects with color corrected, contrast enhanced and final enhanced images.

as 3.35% for Group 1, 2.6% for Group 2, 3.95% for Group 3 and 0.79% for Group 4. The PSF or deblurring kernel for each image is determine based on estimated values of σ_{est} to restore the blurred image. The restored images with their color corrected, contrast adjusted and enhanced or fused images of self-collected dataset are shown in FIGURE 11. The image enhancement provided better colors and intensities that highlighted the degree of corrosion in each pattern more prominently. Especially, the regions of interest, such as the white (non-corroded), light brown (moderately corroded) and dark-brown (highly corroded) areas are enhanced quite well. These enhanced areas made the corrosion estimation process more accurate and easy. It helps in the evaluation of the method for corrosion estimation in the blurry environment. From visual inspection of the enhanced images, it is observed that color and contrast enhancement have been done even in extremely blurred images. It further motivated to test the proposed method on natural underwater images with real blurring, color distortion, and low contrast issues.

Upon executing all restoration and enhancement operations on self-acquired images, the image quality evaluation is performed using full referenced metric. The quality of the final restored and enhanced images in all four groups is evaluated using input or original images as references and results are shown in Table 1. The overall trend of the MSE values in all four groups shows that the blurring effects in the underwater imaging are directly proportional to the MSE as the error increased with higher blurring level. The PSNR is noticed between 25dB and 27dB which reflects that algorithm maintained the quality of the images in all four

TABLE 1. The mean statistical quantities of referenced quality evaluation metric on self-collected underwater images in all four blurring groups.

	MSE	PSNR	SSIM	Entropy Comparison	
				$^{*}MoE_{O}$	$^{**}MoE_{E}$
Group 1	578.26	26.81	0.49	7.37	7.90
Group 2	732.38	25.73	0.42		7.89
Group 3	759.36	25.54	0.39		7.87
Group 4	766.47	25.47	0.37		7.84

$^{*}MoE_{H}$ = Measure of Entropy on original Image
$^{**}MoE_{E}$ = Measure of Entropy on Enhanced Image

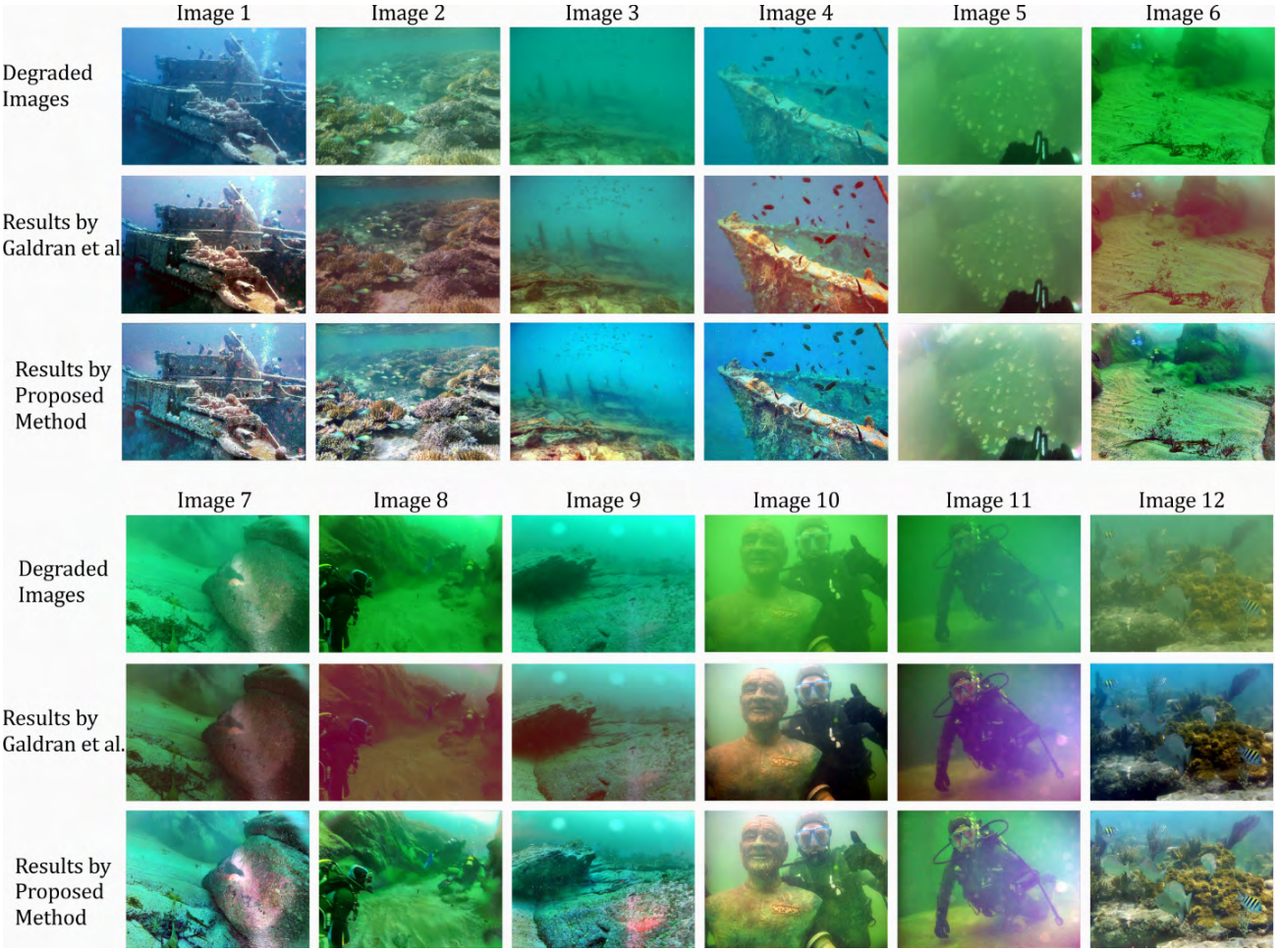

FIGURE 12. The results comparison of proposed method on natural hazy and blurred underwater images with Galdran *et al*. [26].

groups. The SSIM is decreased with blurring effects up to 0.37 and approximately 30 to 50% of an image is maintained in term of luminance, contrast, and structure as compare with the original image. The overall trend of MoE shows that the measured quantity is improved in numbers as compared to input images. This improvement is significant for feature enhancement of the images. The higher values of MoE in all four groups also depict that even with higher blurring effects, the proposed method improved the features of the image.

After obtaining the results on self-collected dataset, the proposed method is validated by comparing the results with existing technique on real underwater images. Due to the limitation of the availability of real underwater image dataset, the validation is performed on few real underwater images as shown in FIGURE 12 that have been used in [26]. These images are severely degraded by underwater effects and have natural blur, low contrast and attenuated colors around the scene that posed a challenge for proposed method to improve them.

The results are compared, both visually and quantitatively with the existing technique proposed by Galdran *et al*. [26]. For comparative analysis, the results of the Galdran *et al*. [26] in term of processed images are downloaded from their available online resource [53]. For a visual comparison, the results on hazy underwater images by Galdran *et al*. [26] and by the proposed method are given in FIGURE 12. From the visual analysis, the proposed method outperforms as compared to Galdran *et al.* [26], however, the dominated color (green) in some of the images such as Image 6, 8 and 10 (see FIGURE 12) are not recovered fully by the proposed method.

For quantitative comparison, the full referenced quality evaluation metric is calculated. The statistical quantities of the metric for both methods are given in Table 2. The overall low MSE and higher PSNR are noticed by the proposed method. The SSIM shows improved numbers in the proposed method which means that the proposed technique can maintain the structure of the image during image restoration process. Similarly, the MoE is also increased, and higher values are achieved in our case which displays that our method has improved the features of the image.

For a quantitative analysis on real underwater hazy images, apart from full referenced metric, the visible edge based evaluation metric (which is used by Galdran *et al.* [26]) is

TABLE 2. The statistical quantities of referenced quality evaluation metric on publicly available hazy underwater images.

	MSE		PSNR		SSIM		Entropy Comparison		
	Galdran et al. [26]	Proposed Method	Galdran et al. [26]	Proposed Method	Galdran et al. [26]	Proposed Method	*MoE $_H$	**MoE $_E$	
								Galdran et al. [26]	Proposed Method
Image1	835.48	535.28	25.22	27.38	0.31	0.63	7.80	7.88	7.83
Image2	635.50	521.58	27.46	27.10	0.10	0.59	7.30	6.96	7.79
Image3	411.61	920.84	30.16	25.34	0.66	0.70	6.57	6.91	7.24
Image4	1744.87	514.51	24.85	27.54	0.06	0.79	6.77	7.17	7.49
Image5	199.44	946.61	34.48	26.61	0.69	0.61	7.28	7.01	7.56
Image6	1866.59	1874.05	23.98	22.51	0.06	0.47	7.33	6.92	7.62
Image7	987.25	753.40	25.18	25.79	0.17	0.60	7.69	6.85	7.85
Image8	1672.70	577.29	24.20	27.32	0.17	0.75	7.13	6.55	7.52
Image9	858.72	816.12	27.84	26.35	0.31	0.69	7.55	7.20	7.63
Image10	1224.52	1053.31	23.32	25.07	0.30	0.53	7.60	7.89	7.78
Image11	1233.36	1297.37	23.40	24.65	0.03	0.41	7.37	7.47	7.63
Image12	667.25	464.71	26.01	27.90	0.39	0.53	6.92	7.61	7.59

*MoE $_H$ = Measure of Entropy on hazy Image
**MoE $_E$ = Measure of Entropy on Enhanced Image

TABLE 3. The coefficients of visible edges based quality evaluation metric on publicly available hazy underwater images.

	e		σ (%)		r	
	Galdran et al.[26]	Proposed Method	Galdran et al. [26]	Proposed Method	Galdran et al. [26]	Proposed Method
Image1	1.035	1.686	0.049	0.003	2.650	3.294
Image2	0.556	1.015	0.000	0.003	1.541	3.491
Image3	3.477	24.357	0.000	0.000	1.626	6.511
Image4	1.604	4.298	0.000	0.000	2.286	5.910
Image5	0.858	19.931	0.000	0.000	1.128	7.146
Image6	0.040	1.652	0.000	0.111	1.108	8.569
Image7	0.299	1.383	0.000	0.011	0.845	6.130
Image8	-0.524	6.166	0.000	0.010	0.732	6.953
Image9	0.265	3.822	0.000	0.010	1.096	8.149
Image10	5.036	8.751	0.321	0.000	2.008	3.653
Image11	21.951	35.526	0.000	0.000	2.936	7.627
Image12	1.276	1.782	0.081	0.000	2.202	4.162

TABLE 4. Underwater dehazing evaluation on images in [55] based on pcqi [51] and uciqe [52] metrics.

	He et al. [56]		Ancuti& Ancuti [31]		Drews-Jr [57]		Galdran et al. [26]		Emberton et al. [58]		Ancuti et al. [59]		Ancuti & Vleeschouwer et al. [55]		Proposed method	
	PCQI	UCIQE	PCQI	UCIQE	PCQI	UCIQE	PCQI	UCIQE	PCQI	UCIQE	PCQI	UCIQE	PCQI	UCIQE	PCQI	UCIQE
Shipwreck	1.012	0.565	0.998	0.629	0.649	0.550	0.920	0.646	0.945	0.632	1.131	0.634	1.172	0.632	1.278	0.599
Fish	1.023	0.602	1.047	0.650	0.863	0.623	0.835	0.527	1.156	0.705	1.089	0.669	1.117	0.667	1.255	0.625
Reef1	1.000	0.612	0.963	0.657	1.046	0.649	0.794	0.576	1.078	0.660	0.978	0.655	1.083	0.658	1.261	0.661
Reef2	0.774	0.702	0.899	0.683	0.483	0.659	0.769	0.633	0.607	0.718	0.983	0.718	1.075	0.711	1.252	0.681
Reef3	1.022	0.606	1.123	0.661	0.793	0.620	0.883	0.533	0.943	0.678	1.191	0.705	1.276	0.697	1.265	0.665
Galdran1	1.056	0.593	1.030	0.631	0.749	0.544	0.507	0.529	1.147	0.652	1.125	0.643	1.152	0.659	1.319	0.632
Galdran2	0.983	0.426	1.016	0.558	0.864	0.536	1.158	0.596	1.136	0.630	1.123	0.667	1.192	0.633	1.238	0.578
Ancuti1	0.860	0.485	1.032	0.561	0.909	0.499	0.962	0.641	1.036	0.499	1.074	0.558	1.022	0.594	1.273	0.542
Ancuti2	0.649	0.456	1.077	0.595	0.475	0.492	0.591	0.529	0.603	0.529	1.015	0.590	0.914	0.592	1.224	0.535
Ancuti3	1.071	0.577	1.071	0.643	0.973	0.535	1.021	0.614	1.129	0.555	1.171	0.652	1.207	0.664	1.302	0.609
Average	0.945	0.562	1.026	0.627	0.780	0.571	0.844	0.582	0.978	0.626	1.088	0.647	1.121	0.651	1.267	0.613

also calculated. Three coefficients of the metric are computed for both methods. These coefficients are calculated by using the Matlab source code available at online resource [54] of Hautière *et al*. [50] and are tabulated in Table 3. The coefficient σ that determines the number of saturated pixels to black and white is almost zero for both cases while other two coefficients e and r show that the higher values are obtained for the proposed method. From both visual and quantitative analyses, it can be concluded that the performance of the proposed method is better than the existing method proposed by Galdran *et al.* [26].

For a broader spectrum of performance comparison, we also conducted an assessment using human visual perception based image quality evaluation metrics PCQI [51] and UCIQE [52]. We applied the proposed approach on the same set of images as presented in [55] for comparison and acquired PCQI and UCQIE metric values. Table 4 presents PCQI and UCIQE metric values for

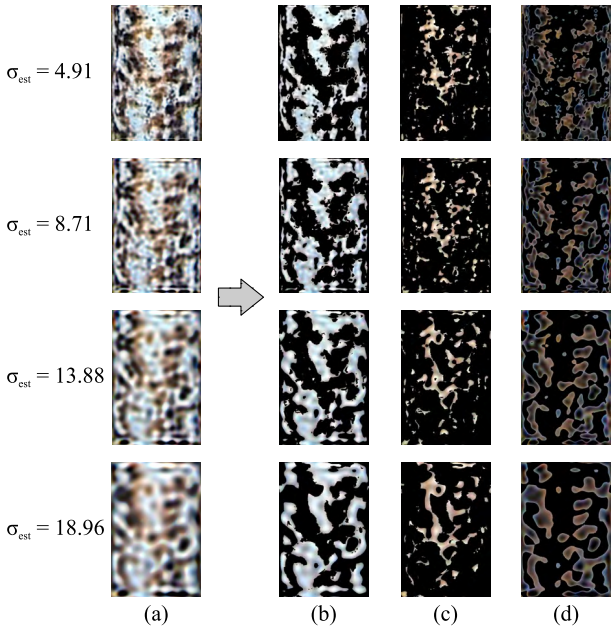

FIGURE 13. (a) The restored and enhanced image of different blurring levels with its (b) non-corroded, (c) moderately corroded and (d) highly corroded clusters.

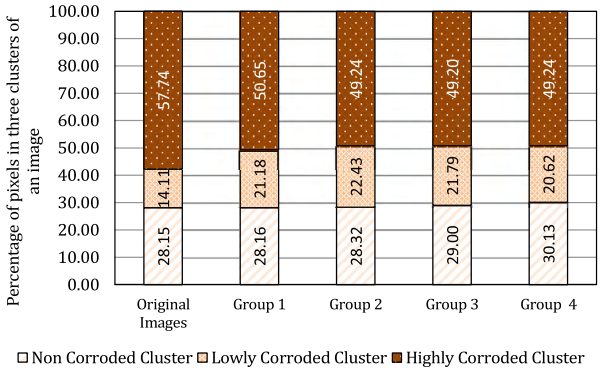

FIGURE 14. The mean percentage of pixels in three clusters of original and all four groups of images.

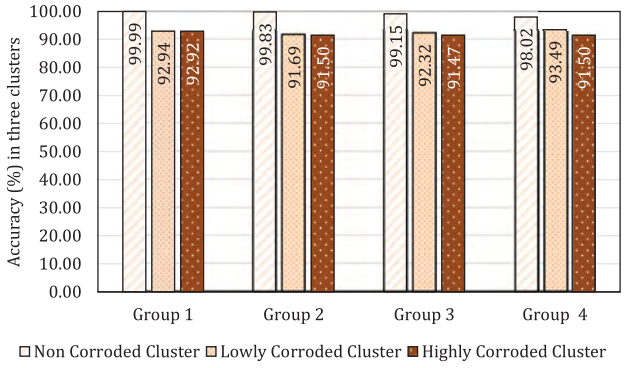

FIGURE 15. The accuracy (%) of pixel counts in each cluster with respect to original image.

a number of recent approaches for underwater image enhancement [26], [31], [55]–[59] as well as our proposed approach. It is noted that the proposed method resulted in compatible values. In particular, in terms of PCQI the proposed method outperformed all the methods with highest average value.

C. CORROSION ESTIMATION

For corrosion estimation, the region of interest is categorized into three clusters. The first cluster consists of the non-corroded region which is represented by white pixels; the second cluster is named as moderately corroded which comprises of light brown pixels while the third cluster consists of dark-brown pixels that are highly corroded part on the surface of the pipe. In order to distinguish between these three different regions, we have adopted unsupervised k-means based clustering approach to group them into three clusters.

The color components of *CIELab* color space are used to segment each cluster based on the above mentioned three colors. In FIGURE 13, the results of k-means based clustering of corroded pipe are presented. From the visual analysis, it is observed that color-based clustering is successful but precision has slightly declined in the images that are restored and enhanced from higher blurring effects. However, the region of interest is accurately portioned into three desired clusters in all four cases.

After extracting three clusters of all the images, the number of pixels in each cluster are estimated. The sum of pixel counts in two clusters; moderately corroded and highly corroded gave the corrosion estimation. This estimation performed on input or original images as well as on all restored and enhanced images of four blurring groups. Due to different pattern of corrosion, each image depicts different percentage of pixels in three clusters. The percentage in each cluster is calculated based on the number of pixels in that cluster with respect to total pixels in the region of interest or the size of the region of interest which is about 480 × 720 pixels. The results of non-corroded, moderately corroded and highly corroded regions in terms of mean percentage of all four groups as well as of original images are shown in FIGURE 14. The results of the mean percentage of non-corroded clusters for all groups including the original images are calculated up to 30.13%. In moderately corroded clusters of original images, the mean percentage of pixels in the region is calculated about 14% while in other four processed groups of images it is found to be between 21 to 23%. Similarly, in the highly-corroded clusters, the original images show about 58% affected region while enhanced images display the mean affected area between 49% and 51%. As in corrosion estimation, only moderately and highly corroded clusters are considered. The accuracy of underwater corossion estimation was caculated using the ground truth images taken in lab environment out of the water. The mean error in these two clusters is calculated about 6% to 9%. The accuracy of corrosion estimation in each cluster of four groups with respect to ground truth images is calculated more than 90% as

TABLE 5. Standard 24 colors patches of ground truth, underwater image and enhanced image with color distance metric.

Colour Name	Ground Truth (GT) Color Patch	Underwater (UW) Colour Patch	Enhanced (EN) Colour Patch	GT vs UW (ΔE)	GT vs EN (ΔE)
dark-skin				21.90	16.18
light-skin				26.03	11.97
blue-sky				26.32	15.50
foliage				16.28	13.66
blue-flower				26.94	13.35
bluish-green				19.97	8.01
orange				33.02	20.73
purplish-blue				26.47	15.24
moderate-red				35.09	22.56
purple				21.49	12.42
yellow-green				17.10	5.79
orange-yellow				29.66	14.91
blue				25.21	13.94
green				9.98	5.63
red				33.14	20.83
yellow				33.97	19.76
magenta				30.58	18.04
cyan				25.80	14.98
white				32.62	17.20
neutral-8				27.75	14.57
neutral-6.5				22.78	11.80
neutral-5				21.54	13.28
neutral-3.5				19.17	13.07
black				16.13	10.28

shown in FIGURE 15. The less error with higher accuracy in cluster-based corrosion estimation proves the overall performance of the proposed method in four groups of images having different blurring effects.

D. COLOR DIFFERENCE EVALUATION EXPERIMENT

In this study, the color is an important feature to estimate the corrosion of the pipeline, so it is essential to evaluate the proposed method for color enhancement. Therefore, besides conventional image quality evaluation metrics as described in section A.1, an experiment was conducted to calculate color distance metric. A color checker (as shown in FIGURE 16(a)) was developed with 24 standard color patches using Color Checker Passport by X-Rite [34]. Two images of the developed color checker were taken (one in underwater and other out of water as a ground truth) under normal illumination conditions as shown in FIGURE 16 (a) & (b). In both cases, the distance from the color checker to the camera

(a) (b) (c)

FIGURE 16. Color checker with 24 standard colors. (a) Ground truth image (b) underwater hazy image (c) restored and enhanced underwater image.

was kept similar at about 1.5 meters. Then the underwater image was processed through proposed image restoration and enhancement algorithm to improve the image (see FIGURE 16 (c)). Then all 24 color patches are cropped from each of the image (i.e. ground truth, underwater and enhanced image) as given in Table 4. All the patches from each image are converted from RGB to *CIELab* color space to calculate the difference metric ΔE by using L, a and b values of ground truth, underwater image and enhanced image as given in Eqn. (15).

$$\Delta E(GT, I) = \sqrt{(L_{GT} - L_I)^2 + (a_{GT} - a_I)^2 + (b_{GT} - b_I)^2} \tag{15}$$

where GT and I are the ground truth and input image, respectively. In our case, the underwater and enhanced images are considered as input images.

The quantitative analysis of the color patches shows better performance of the proposed method in terms of low values of for enhanced image as compared hazy underwater image. From the visual analysis, it is also observed that the colors patches are severely degraded in hazy underwater image however the proposed method has improved each color patch in enhanced image as shown in Table 4. The performance of proposed method in this experiment authenticated the color-based corrosion estimation.

V. CONCLUDING REMARKS

This paper presented a new image-based methodology for subsea pipeline corrosion estimation. The image restoration and enhancement prior to corrosion estimation was tested on self-collected as well as on publicly available degraded underwater image datasets, both have shown promising results. A high accuracy of more than 90% is achieved for corrosion estimation in all three defined clusters for different underwater blurring conditions. As the corrosion estimation is based on color information of the corroded pipe; therefore, besides conventional image quality evaluation metrics, a color distance experiment was conducted. The color distance metric (ΔE) depicts improved performance of the proposed method in terms of low values as compared to hazy underwater image. At present, the presented method can estimate only the corroded surface area of the pipe; however, in future the method will be improved to estimate the depth of the effected region as well. Present improved results suggested to integrate the proposed method into an underwater robotic system for real-time inspection and monitoring of actual subsea pipeline corrosion inspection activities.

REFERENCES

[1] J. Franklin. *Subsea Pipeline Inspection, Repair and Maintenance*. Accessed: Apr. 16, 2017. [Online]. Available: http://www.theonltd.com/news/subsea-pipeline-inspection-repair-and-maintenance/

[2] R. Norsworthy, "Understanding corrosion in underground pipelines: Basic principles," in *Underground Pipeline Corrosion*. Amsterdam, The Netherlands: Elsevier, 2014, pp. 3–34.

[3] *Integrity Management of Submarine Pipeline Systems*, DNV GL, 2009.

[4] U. Ewert *et al.*, "Corrosion monitoring with tangential radiography and limited view computed tomography," in *Proc. AIP Conf.*, vol. 1706. Berlin, Germany: BAM Federal Institute for Materials Research and Testing, 2016, p. 110003.

[5] M. I. Haith *et al.*, "Modelling based radiography for NDE of subsea pipelines," in *Proc. AIP Conf.*, vol. 1706, no. 1, 2016, pp. 110004–160002.

[6] D. S. Forsyth, *Non-Destructive Testing for Corrosion*. Austin, TX, USA: Texas Research International, ch. 21, pp. 1–12.

[7] L. Cartz, *Nondestructive Testing: Radiography, Ultrasonics, Liquid Penetrant, Magnetic Particle, Eddy Current*. Russell Township, OH, USA: ASM International, 1995.

[8] R. A. Quinn and C. C. Sigl, Eds., *Radiography in Modern Industry*, 4th ed. New York, NY, USA: Eastman Kodak Company Rochester, 1980.

[9] *NDT Resource Center*. Accessed: Apr. 17, 2017. [Online]. Available: https://www.nde-ed.org/EducationResources/CommunityCollege/NDTIntro/cc_intro001.htm

[10] E. Lange, S. Petersen, L. Rüpke, E. Söding, and K. Wallmann, "Marine resources—Opportunities and risks," in *World Ocean Review*, no. 3. Hamburg, Germany: Maribus, 2014.

[11] A. Bagnitsky, A. Inzartsev, A. Pavin, S. Melman, and M. Morozov, "Side scan sonar using for underwater cables & pipelines tracking by means of AUV," in *Proc. IEEE Symp. Underwater Technol. Workshop Sci. Use Submarine Cables Rel. Technol.*, Apr. 2011, pp. 1–10.

[12] T. Szyrowski, S. K. Sharma, R. Sutton, and G. A. Kennedy, "Developments in subsea power and telecommunication cables detection: Part 1—Visual and hydroacoustic tracking," *Int. J. Soc. Underwater Technol.*, vol. 31, no. 3, pp. 123–132, Jul. 2013.

[13] A. Ortiz, J. Antich, and G. Oliver, "A particle filter-based approach for tracking undersea narrow telecommunication cables," *Mach. Vis. Appl.*, vol. 22, no. 2, pp. 283–302, Mar. 2011.

[14] *Analysis of Material's Corrosion Through Image Processing Analysis of Material's Corrosion Through Image Processing by Rogue Wave Software*, Rogue Wave Software, Boulder, CO, USA, 2011.

[15] S. Yammen, S. Bunchuen, U. Boonsri, and P. Muneesawang, "Pole tip corrosion detection using various image processing techniques," in *The Era of Interactive Media*. New York, NY, USA: Springer, 2013, pp. 423–431.

[16] F. Bonnín-Pascual and A. O. Rodriguez, "Corrosion detection for automated visual inspection," in *Developments in Corrosion Protection*. Rijeka, Croatia: InTech, 2014.

[17] N. A. Zulkifli, K. S. M. Sahari, A. Anuar, and M. A. Aziz, *Corrosion Detection Using LabVIEW for Robotic Inspection of Boiler Headers*. Singapore: Springer, 2014, pp. 31–37.

[18] M. Motamedi, F. Faramarzi, and O. Duran, "New concept for corrosion inspection of urban pipeline networks by digital image processing," in *Proc. 38th Annu. Conf. IEEE Ind. Electron. Soc. (IECON)*, Oct. 2012, pp. 1551–1556.

[19] F. F. Feliciano, F. R. Leta, and F. B. Mainier, "Texture digital analysis for corrosion monitoring," *Corrosion Sci.*, vol. 93, pp. 138–147, Apr. 2015.

[20] M. R. G. Acosta, J. C. V. Díaz, and N. S. Castro, "An innovative image-processing model for rust detection using Perlin Noise to simulate oxide textures," *Corrosion Sci.*, vol. 88, pp. 141–151, Nov. 2014.

[21] J. Y. Chiang and Y.-C. Chen, "Underwater image enhancement by wavelength compensation and dehazing," *IEEE Trans. Image Process.*, vol. 21, no. 4, pp. 1756–1769, Apr. 2012.

[22] C. Li and J. Guo, "Underwater image enhancement by dehazing and color correction," *J. Electron. Imag.*, vol. 24, no. 3, p. 033023, 2015.

[23] C.-Y. Cheng, C.-C. Sung, and H.-H. Chang, "Underwater image restoration by red-dark channel prior and point spread function deconvolution," in *Proc. IEEE Int. Conf. Signal Image Process. Appl. (ICSIPA)*, vol. 1, Oct. 2016, pp. 110–115.

[24] B. L. McGlamery, "A computer model for underwater camera systems," *Proc. SPIE*, vol. 208, pp. 221–231, Mar. 1980.

[25] J. S. Jaffe, "Computer modeling and the design of optimal underwater imaging systems," *IEEE J. Ocean. Eng.*, vol. 15, no. 2, pp. 101–111, Apr. 1990.

[26] A. Galdran, D. Pardo, A. Picón, and A. Alvarez-Gila, "Automatic red-channel underwater image restoration," *J. Vis. Commun. Image Represent.*, vol. 26, pp. 132–145, Jan. 2015.

[27] K. He, J. Sun, and X. Tang, "Single image haze removal using dark channel prior," *IEEE Trans. Pattern Anal. Mach. Intell.*, vol. 33, no. 12, pp. 2341–2353, Dec. 2011.

[28] Y.-T. Peng and P. C. Cosman, "Underwater image restoration based on image blurriness and light absorption," *IEEE Trans. Image Process.*, vol. 26, no. 4, pp. 1579–1594, Apr. 2017.

[29] Y. Li, Y. Zhang, X. Xu, L. He, S. Serikawa, and H. Kim, "Dust removal from high turbid underwater images using convolutional neural networks," *Opt. Laser Technol.*, to be published.

[30] H. Lu, Y. Li, H. Kim, and S. Serikawa, "Underwater light field depth map restoration using deep convolutional neural fields," in *Artificial Intelligence and Robotics* (Studies in Computational Intelligence), vol. 752. Cham, Switzerland: Springer, 2018, pp. 305–312.

[31] C. O. Ancuti and C. Ancuti, "Single image dehazing by multi-scale fusion," *IEEE Trans. Image Process.*, vol. 22, no. 8, pp. 3271–3282, Aug. 2013.

[32] M. Han, Z. Lyu, T. Qiu, and M. Xu, "A review on intelligence dehazing and color restoration for underwater images," *IEEE Trans. Syst., Man, Cybern. Syst.*, vol. 1, no. 1, pp. 1–13, Jan. 2018, doi: 10.1109/TSMC.2017.2788902.

[33] J. Flusser, S. Farokhi, C. Höschl, T. Suk, B. Zitová, and M. Pedone, "Recognition of images degraded by Gaussian blur," *IEEE Trans. Image Process.*, vol. 25, no. 2, pp. 790–806, Feb. 2016.

[34] A. Khan, "Underwater image enhancement and dehazing for subsea pipeline corrosion inspection," Univ. Teknol. Petronas, Seri Iskandar, Malaysia, Tech. Rep. 1, 2017.

[35] R. C. Gonzalez, R. E. Woods, and S. L. Eddins, *Digital Image Processing Using MATLAB*. London, U.K.: Dorsing Kindersley, 2004.

[36] A. S. A. Ghani and N. A. M. Isa, "Underwater image quality enhancement through composition of dual-intensity images and Rayleigh-stretching," *SpringerPlus*, vol. 3, no. 1, p. 757, 2014.

[37] S. M. Pizer, "Adaptive histogram equalization and its variations," *Comput. Vis., Graph., Image Process.*, vol. 39, no. 3, pp. 355–368, 1987.

[38] D. J. Ketcham, R. W. Lowe, and J. W. Weber, *Image Enhancement Techniques for Cockpit Displays*. Fort Belvoir, VA, USA: Defense Technical Information Center, 1974.

[39] R. Hummel, "Image enhancement by histogram transformation," *Comput. Graph. Image Process.*, vol. 6, no. 2, pp. 184–195, 1977.

[40] K. Zuiderveld, *Contrast Limited Adaptive Histogram Equalization*, G. Graphics and P. S. Heckbert, Eds. San Diego, CA, USA: Academic, 1994, pp. 474–485.

[41] U. Qidwai and C. H. Chen, *Digital Image Processing: An Algorithmic Approach With MATLAB*, 1st ed. London, U.K.: Chapman & Hall, 2009.

[42] R. J. Medina-Daza, N. E. Vera-Parra, and E. Upegui, "Wavelet daubechies (db4) transform assessment for WorldView-2 images fusion," *J. Comput.*, vol. 12, no. 4, pp. 301–308, 2017.

[43] J.-H. Park, R. Tateishi, and K. Wikantika, "Multisensor data fusion using multiresolution analysis (MRA)," *Int. Arch. Photogramm. Remote Sens.*, vol. 33, pp. 430–437, Jul. 2000.

[44] R. R. Fessler, "Pipeline corrosion," U.S. Dept. Transp. Pipeline Hazard, USA, Tech. Rep. DTRS56-02-D-70036, Nov. 2008.

[45] S. Lloyd, "Least squares quantization in PCM," *IEEE Trans. Inf. Theory*, vol. IT-28, no. 2, pp. 129–137, Mar. 1982.

[46] R. C. Gonzalez and R. E. Woods, *Digital Image Processing*. Upper Saddle River, NJ, USA: Prentice-Hall, 2008.

[47] Z. Wang, A. C. Bovik, H. R. Sheikh, and E. P. Simoncelli, "Image quality assessment: From error visibility to structural similarity," *IEEE Trans. Image Process.*, vol. 13, no. 4, pp. 600–612, Apr. 2004.

[48] E. A. Silva, K. Panetta, and S. S. Agaian, "Quantifying image similarity using measure of enhancement by entropy," *Proc. SPIE*, vol. 6579, p. 65790U, May 2007.

[49] J.-P. Tarel and N. Hautiere, "Fast visibility restoration from a single color or gray level image," in *Proc. IEEE 12th Int. Conf. Comput. Vis.*, Sep./Oct. 2009, pp. 2201–2208.

[50] N. Hautière, J.-P. Tarel, D. Aubert, and É. Dumont, "Blind contrast enhancement assessment by gradient ratioing at visible edges," *Image Anal. Stereol. J.*, vol. 27, no. 2, pp. 87–95, Jun. 2008.

[51] S. Wang, K. Ma, H. Yeganeh, Z. Wang, and W. Lin, "A patch-structure representation method for quality assessment of contrast changed images," *IEEE Signal Process. Lett.*, vol. 22, no. 12, pp. 2387–2390, Dec. 2015.

[52] M. Yang and A. Sowmya, "An underwater color image quality evaluation metric," *IEEE Trans. Image Process.*, vol. 24, no. 12, pp. 6062–6071, Dec. 2015.

[53] A. Galdran. *Galdran Underwater Dataset*. Accessed: Dec. 1, 2016. [Online]. Available: https://github.com/agaldran/UnderWater

[54] N. Hautière. *MATLAB Source Code*. Accessed: Dec. 1, 2016. [Online]. Available: http://perso.lcpc.fr/tarel.jean-philippe/publis/ics07.html

[55] C. O. Ancuti, C. Ancuti, C. De Vleeschouwer, and P. Bekaert, "Color balance and fusion for underwater image enhancement," *IEEE Trans. Image Process.*, vol. 27, no. 1, pp. 379–393, Jan. 2018.

[56] K. He, J. Sun, and X. Tang, "Single image haze removal using dark channel prior," *IEEE Trans. Pattern Anal. Mach. Intell.*, vol. 33, no. 12, pp. 2341–2353, Dec. 2011.

[57] P. Drews, Jr., E. do Nascimento, F. Moraes, S. Botelho, and M. Campos, "Transmission estimation in underwater single images," in *Proc. IEEE Int. Conf. Comput. Vis. Workshops*, Dec. 2013, pp. 825–830.

[58] S. Emberton and L. Chittka, "Hierarchical rank-based veiling light estimation for underwater dehazing," in *Proc. BMV*, 2015, pp. 1–12.

[59] C. Ancuti, C. O. Ancuti, T. Haber, and P. Bekaert, "Enhancing underwater images and videos by fusion," in *Proc. IEEE Conf. Comput. Vis. Pattern Recognit.*, Jun. 2012, pp. 81–88.

AMJAD KHAN received the bachelor's degree in electronic engineering from Iqra University, Karachi, Pakistan, in 2014, and the master's degree in electrical and electronics engineering by research from Universiti Teknologi PETROAS, Malaysia. He has served the industry for many years under different capacities. He is currently with the Centre for Intelligent Signal and Imaging Research, Universiti Teknologi PETROAS. His interests include image processing, visual surveillance, computer vision, machine learning, deep learning, and medical image analysis.

SYED SAAD AZHAR ALI (M'07–SM'17) received the B.E. degree in electrical engineering from NED University, Karachi, Pakistan, and the master's and Ph.D. degrees in nonlinear control from the King Fahd University of Petroleum and Minerals. He was with Air University and Iqra University. He is currently an Associate Professor with the Center of Intelligent Signal and Imaging Research, Universiti Teknologi PETRONAS, Malaysia. He leads the Visual Surveillance and Monitoring Group. Recently, he has been involved in neurosignal processing. He has authored over 70 peer-reviewed publications, including four books/chapters. His research focuses on intelligent control, signal processing, underwater robotics with the emphasis on image enhancement, and 3-D scene reconstruction. He is a PI for several funded research projects.

ATIF ANWER received the bachelor's degree in mechatronics engineering from the National University of Sciences and Technology, Islamabad, Pakistan, in 2004, and the master's degree in electrical and electronics engineering by research from Universiti Teknologi PETRONAS, Malaysia. He has a background in robot vision, embedded systems, mechanical design, additive manufacturing, and control system design and implementation. He is currently with the Centre for Intelligent Signal and Imaging Research, Universiti Teknologi PETROAS. His interests include mobile robotics, robot and machine vision, and underwater robotics.

SYED HASAN ADIL received the Ph.D. degree in computer science from Iqra University, Pakistan. He is currently an Associate Professor and the Chair of the Software Engineering Department, Iqra University. He has authored or co-authored several research papers in national and international journals and conferences. His area of research includes machine learning, optimization, parallel computing, and data science.

FABRICE MÉRIAUDEAU was born in Villeurbanne, France, in 1971. He received the master's degree in physics, the Engineering degree (Hons.) in material sciences, and the Ph.D. degree in image processing from Dijon University, France, in 1994 and 1997, respectively. He held a post-doctoral position with the Oak Ridge National Laboratory for a year. He was the Director of the Laboratoire Electronique, Informatique et Image, UMR CNRS, which has more than 200 staff members, from 2011 to 2016. He was a Coordinator of the Erasmus Mundus Master degree in the field of computer vision and robotics from 2006 to 2010. He was the Vice President for International Affairs with the University of Burgundy from 2010 to 2012. Since 2016, he has been a Professor with Universiti Teknologi PETRONAS. He has authored or co-authored over 150 international publications and holds three patents. His research interests focused on image processing for non-conventional imaging systems (UV, IR, and polarization) and more recently on medical/biomedical imaging.